Published in final edited form as:

Neurobiol Aging. 2020 March ; 87: 89–97. doi:10.1016/j.neurobiolaging.2019.11.016.

Characterization of Age-related Microstructural Changes in Locus Coeruleus and Substantia Nigra Pars Compacta

Jason Langley[1], **Sana Hussain**[2], **Justino J. Flores**[3], **Ilana J. Bennett**[3], **Xiaoping Hu**[1,2,*]

[1]Center for Advanced Neuroimaging, University of California Riverside, Riverside, CA

[2]Department of Bioengineering, University of California Riverside, Riverside, CA

[3]Department of Psychology, University of California Riverside, Riverside, CA

Abstract

Locus coeruleus (LC) and substantia nigra pars compacta (SNpc) degrade with normal aging, but not much is known regarding how these changes manifest in MRI images, or whether these markers predict aspects of cognition. Here, we use high-resolution diffusion-weighted MRI to investigate microstructural and compositional changes in LC and SNpc in young and older adult cohorts, as well as their relationship with cognition. In LC, the older cohort exhibited a significant reduction in mean and radial diffusivity, but a significant increase in fractional anisotropy compared to the young cohort. We observed a significant correlation between the decrease in LC mean, axial, and radial diffusivities and measures examining cognition (Rey Auditory Verbal Learning Test delayed recall) in the older adult cohort. This observation suggests that LC is involved in retaining cognitive abilities. In addition, we observed that iron deposition in SNpc occurs early in life and continues during normal aging.

Keywords

Locus coeruleus; DTI; aging; substantia nigra; iron deposition

1. Introduction

Locus coeruleus (LC) and substantia nigra pars compacta (SNpc) are catecholamine nuclei situated in brainstem and subcortex, respectively. They both consist of neuromelanin generating catecholaminergic neurons and can be delineated in neuromelanin-sensitive MRI images (Chen et al., 2014; Sasaki et al., 2006; Schwarz et al., 2011). Both nuclei are thought

*Correspondence to: Xiaoping P. Hu, Ph.D., Provost Fellow, Professor and Chair Department of Bioengineering, University of California, Riverside, Materials Science and Engineering 205, Phone: (951) 827-2925, Fax: (951) 827-6416, xhu@engr.ucr.edu.

The authors have no conflicts of interest and are all employed by the University of California, Riverside.

The data contained in the manuscript being submitted have not been previously published and is not under consideration for publication elsewhere.

Written, informed consent was obtained from all subjects prior to participation in the study.

to play prominent roles in cognition. Specifically, LC plays a major role in arousal, attention modulation, and memory (Aston-Jones, Gary and Cohen, Jonathan D., 2005; Carter et al., 2010), and SNpc participates in motor function, novelty processing, and temporal processing (Jahanshahi et al., 2006). Loss of melanized neurons in one or both nuclei is known to occur in age-related disorders, including Alzheimer's disease (Braak et al., 2011) and Parkinson's disease (PD) (Braak et al., 2003). However, less is known about how these regions are affected in normal aging.

Histological studies have revealed that both LC and SNpc undergo neuronal loss or compositional changes in normal aging. Approximately 40% of LC neurons are lost by age 40 (Manaye et al., 1995) while neuronal loss in SNpc is estimated to occur at a rate of approximately 4.7% per decade of life (Fearnley and Lees, 1991). These microstructural differences can be examined *in vivo* with diffusion imaging, which measures the movement of molecular water (Beaulieu, 2002). Measures such as the degree of restricted diffusion (fractional anisotropy, FA) are sensitive to altered microstructural "integrity" (e.g., degeneration or demyelination), particularly in highly aligned white matter. The average (mean diffusivity, MD) or perpendicular (radial diffusivity, RD) rates of diffusion may instead capture microstructural differences in gray matter, such as the catecholamine nuclei of interest here. Previous studies in aging have shown changes in these diffusion metrics in deep gray matter structures (e.g., putamen, globus pallidus) in older relative to younger (Pfefferbaum et al., 2010).

To date, however, few studies have examined compositional and microstructural changes in substantia nigra localized by neuromelanin-sensitive MRI and no studies have assessed microstructural changes in LC using diffusion tensor imaging (DTI). One reason may be that assessment of catecholamine nuclei microstructure is hampered by the low resolution of diffusion-weighted images, which is typically insufficient to resolve LC. Furthermore, as SNpc experiences age-related iron deposition in addition to neuronal loss (Hallgren and Sourander, 1958), SNpc diffusion metrics might be influenced by age-related iron accumulations in SNpc. Specifically, iron reduces diffusivity values (Zhong et al., 1991) in diffusion-weighted acquisitions using monopolar diffusion encoding gradients (Fujiwara et al., 2014).

Iron deposition can be measured using quantitative susceptibility mapping (QSM) or R_2* (Langkammer et al., 2012). In substantia nigra, age-related changes in iron (Aquino et al., 2009; Bilgic et al., 2012; Haacke et al., 2010; Pfefferbaum et al., 2009) and microstructure (Pfefferbaum et al., 2010; Vaillancourt et al., 2012) have been assessed using regions of interest (ROIs) placed in T_2-weighted images (Aquino et al., 2009; Bilgic et al., 2012; Haacke et al., 2010; Pfefferbaum et al., 2009). However, these ROIs are mostly spatially incongruent to the neuromelanin-sensitive substantia nigra (i.e. SNpc) (Langley et al., 2015) and, to date, age-related iron deposition or microstructural alterations have not been examined in SNpc defined by neuromelanin-sensitive MRI.

The current study takes advantage of recent advances in MRI hardware and acquisition strategies that have allowed for diffusion imaging with sub-millimeter in plane resolution, suitable for imaging LC. In this work, we will examine age-related microstructural and

compositional differences in the catecholamine nuclei (LC, SNpc) using a combination of diffusion imaging and QSM/R_2*. In addition, we assess the influence of iron on diffusion measures from diffusion-weighted sequences using monopolar and bipolar diffusion encoding gradients. The functional impact of these age-related structural differences are further ascertained in relation to memory performance.

2. Materials and Methods

Sixty-one participants (24 older and 37 young participants) enrolled in this study. Participants in the older adult cohort were recruited from the Riverside community and participants in the young cohort were recruited from the student population at University of California-Riverside. Participants were excluded from the study if there were any contraindications to MRI imaging or if they had a diagnosed neurological condition. All participants in the study gave written informed consent in accordance with local institutional review board (IRB) regulations. One young participant was excluded from the diffusion-weighted MRI analysis due to problems with data acquisition and three participants (2 older adult and 1 young) were excluded from the analyses because of significant motion artifacts. The final sample size used in the analysis was 22 older adult participants and 35 participants in the young cohort. Demographic information (gender, age) and Montreal cognitive assessment scoring (MOCA) and Rey Auditory Verbal Learning Test (RAVLT) scores were collected on each participant. Group means for Age, MOCA, and RAVLT scores are given in Table 1.

2.1 Image Acquisition

Imaging data were acquired on a 3 T MRI scanner (Prisma, Siemens Healthineers, Malvern, PA) using a 32-channel receive only coil at the Center for Advanced Neuroimaging at University of California-Riverside. Anatomic images were acquired with an MP-RAGE sequence (echo time (TE)/repetition time (TR)/inversion time=3.02/2600/800 ms, flip angle=8°, voxel size=0.8×0.8×0.8 mm^3) for registration from subject space to common space. Multi-echo data were collected with a 12 echo 3D gradient recalled echo (GRE) sequence: $TE_1/\Delta TE/TR$ = 4/3/40 ms, FOV = 192 × 224 mm^2, matrix size of 192×224×96, slice thickness=1.7 mm, GRAPPA acceleration factor=2. Magnitude and phase images were saved for R_2* calculation and QSM processing, respectively. High-resolution diffusion-weighted MRI data were collected with a diffusion-weighted single-shot spin-echo, echo planar imaging sequence with the following parameters: TE / TR = 78 / 4500 ms, FOV = 194 × 168 mm^2, matrix size of 204 × 176, voxel size = 0.95 × 0.95 × 1 mm^3, multiband factor = 2, 64 slices with no gap, covering the brain from the middle of the cerebellum to the striatum. A monopolar diffusion encoding gradient was used to generate diffusion weighting. Diffusion-weighting gradients were applied in 30 directions with b values of 500 s/mm^2 and 2000 s/mm^2 with 32 b=0 images. Another set of 32 b=0 images with phase-encoding directions of opposite polarity were acquired to correct for susceptibility distortion (Andersson et al., 2003).

The use of a monopolar diffusion encoding gradient was necessary to achieve spatial resolutions needed to resolve the LC. However, monopolar diffusion encoding gradients are

particularly problematic in structures with elevated iron content, such as substantia nigra. Bipolar diffusion encoding gradients are insensitive to field inhomogeneities generated by iron (Novikov et al., 2018; Zhong et al., 1991). To examine the age-related effects without the influence of iron, an additional lower-resolution diffusion-weighted MRI dataset was collected with bipolar diffusion encoding gradients. Whole brain diffusion-weighted MRI data were collected with a diffusion-weighted single-shot spin-echo, echo planar imaging sequence with the following parameters: TE / TR = 102 / 3500 ms, FOV = 212 × 182 mm^2, matrix size of 128 × 110, voxel size = 1.7 × 1.7 × 1.7 mm^3, multiband factor = 4, 64 slices with no gap. Diffusion-weighting gradients were applied in 64 directions with *b* values of 1500 s/mm^2 and 3000 s/mm^2 with 3 *b*=0 images. For the diffusion-weighted MRI dataset with bipolar diffusion encoding gradients, two sets of diffusion-weighted images with phase-encoding directions of opposite polarity were acquired to correct for susceptibility distortion (Andersson et al., 2003).

2.2 Standard space transformation

Imaging data were analyzed with FMRIB Software Library (FSL). A transformation was derived between individual subject space to Montreal Neurological Institute (MNI) 152 T_1-weighted space using FMRIB's Linear Image Registration Tool (FLIRT) and FMRIB's Nonlinear Image Registration Tool (FNIRT) in the FSL software package using the following steps (Smith et al., 2004; Woolrich et al., 2009). (1) The T_1-weighted image was skull stripped using the brain extraction tool (BET) in FSL, (2) brain extracted T_1-weighted images were aligned with the MNI brain extracted image using an affine transformation, and (3) a nonlinear transformation (FNIRT) was used to generate a transformation from individual T_1-weighted images to T_1-weighted MNI152 common space.

2.3 Neuromelanin-sensitive atlases

A SNpc neuromelanin atlas in MNI 152 space was created for use in this study from a separate cohort of 31 healthy participants (mean age: 26.1 years) using a process similar to those outlined earlier (Langley et al., 2016; Langley et al., 2017). The SNpc template was transferred from MNI 152 space to individual subject space using FLIRT and FNIRT in the FSL software package as follows (Smith et al., 2004; Woolrich et al., 2009). First, brain extracted T_1-weighted images were aligned with the MNI brain extracted image using an affine transformation. Second, a nonlinear transformation was used to generate a transformation from individual subject space to common space. Next, individual SNpc and masks were transformed to their respective T_1-weighted images using FLIRT and then transformed to common space using FNIRT. Finally, the first echo from the T_2-weighted GRE sequence was brain extracted using the brain extraction tool (BET) in FSL and a rigid body transformation was used to register the brain extracted T_1-weighted image with FLIRT. The resulting transformation matrix was used to transform the SNpc mask in T_1-space to T_2-weighted or diffusion space. The resultant SNpc masks were thresholded at a level of 0.6, corresponding to at least 60% of the participants sharing the voxel, and then binarized. Each transformation was checked for errors, and no discemable difference was seen in the location of the ventricles in the T_1-weghted, T_2-weighted, and diffusion images.

An LC atlas was created from the same population used to create the SNpc neuromelanin atlas. LC was segmented using a previously used procedure (Chen et al., 2014), transformed to MNI standard space, and a population map was created using the steps outlined above. The LC atlas was thresholded at a level of 0.6, binarized, and then transformed to individual T_2-weighted or diffusion images as described above. LC and SNpc atlases used in this analysis are shown in Figure 1.

2.4 Diffusion processing

Diffusion-weighted data were analyzed with FSL (Jenkinson et al., 2002; Jenkinson and Smith, 2001; Smith et al., 2004) and MATLAB (The Mathworks, Natick, MA). Standard preprocessing steps were applied to correct susceptibility induced distortions in the diffusion MR data. Diffusion MR data were first corrected for eddy-current distortion, motion, and for susceptibility distortion using eddy in FSL (Andersson et al., 2003; Andersson and Sotiropoulos, 2016). Next, skull stripping of the T_1-weighted image and susceptibility corrected b=0 image was performed using the brain extraction tool in the FSL software package (Smith, 2002). Finally, measures derived from the diffusion MR data, including fractional anisotropy (FA) and mean diffusivity (MD) were calculated using the dtifit tool in FSL. Radial diffusivity (RD) and axial diffusivity (AD) was obtained from the resulting eigenvalue maps. Processing and registration steps are illustrated in Figure 2.

2.5 R_2* and QSM processing

R_2* values were estimated using a custom script in MATLAB by fitting a monoexponential model to the GRE images.

$$S_i = S_0 \exp(-R_2^* TE) \quad [1]$$

where S_0 denotes a fitting constant and S_i denotes the signal of a voxel at the ith echo time. The resulting R_2* map was aligned to the T_1-weighted image using a transform derived via the magnitude image from the first echo (FLIRT, degrees of freedom = 6). For each participant, mean R_2* was measured in the SNpc and in LC ROIs.

QSM images were constructed using the following procedure. Phase maps were constructed from the raw data, and phase offsets were removed. Next, phase maps were unwrapped (Langley and Zhao, 2009). The background phase was then removed with the spherical mean value method using a filter having a radius of eight pixels (Schweser et al., 2011). Finally, susceptibility maps were derived from the frequency map of brain tissue using an improved least-squares (iLSQR) method (Li et al., 2015; Li et al., 2011) and Laplace filtering with a threshold of 0.04 as a truncation value. All QSM images were processed in MATLAB (The Math-Works, Inc., Natick, MA, USA) using in-house scripts. Mean susceptibility was measured in SNpc for each participant. Susceptibility was not measured in LC due to substantial susceptibility artifacts generated by the fourth ventricle.

2.6 Statistical Analysis

All statistical analyses were performed using IBM SPSS Statistics software version 24 (IBM Corporation, Somers, NY, USA) and results are reported as mean ± standard deviation. A p

value of 0.05 was considered significant for all statistical tests performed in this work. Normality of diffusion and iron data was assessed using the Shapiro-Wilk test for each group and all data was found to be normal. Group R_2*, susceptibility, and DTI indices comparisons between the young and older adult cohort were made using separate two-tailed *t*-tests, and we expected group effects in each measure.

Spearman rank correlations of mean SNpc R_2* and mean SNpc susceptibility with age were performed separately in both cohorts. As histology suggests a rapid accrual of iron early in life and leveling off later in life (Hallgren and Sourander, 1958), we expected significant correlations in mean SNpc R_2* and susceptibility in the young cohort but not in the older adult cohort. The dependence of diffusivity on iron content in SNpc was ascertained with Spearman rank correlations between monopolar and bipolar diffusion indices and iron measures (R_2* or susceptibility), in each group. As the bipolar diffusion acquisition is insensitive to magnetic field inhomogeneities generated by iron, we predicted the diffusion indices from the monopolar acquisition would be sensitive to iron but not diffusion indices from the bipolar acquisition.

Older monkeys exhibit deficits in memory (Bartus, 1979) and have decreased catecholaminergic innervation of the prefrontal cortex (Goldman-Rakic and Brown, 1981). In addition, pharmacological manipulation of noradrenaline was found to influence memory in older monkeys (Arnsten and Contant, 1992; Jackson and Buccafusco, 1991). As LC is the primary source of norepinephrine in the brain, we hypothesize that LC impairment, as indicated by microstructural measures, would correlate with RAVLT delayed recall score in the older adult group. Thus, to assess the impact of LC, we performed a correlation between mean LC DTI indices and RAVLT delayed recall scores separately in younger and older adults. Age group differences in the magnitude of these relationships were assessed using one-tailed Fisher's *z* tests for independent correlations.

Dopaminergic neurons in SNpc and ventral tegmental area (VTA) can be directly imaged using magnetization transfer effects (Chen et al., 2014; Sasaki et al., 2006; Schwarz et al., 2011). Magnetization transfer contrast in SNpc and VTA has found to correlate with verbal learning and verbal memory performance in older adults (Duzel et al., 2008). Given the relationship between verbal memory and SNpc/VTA, we hypothesized that SNpc impairment, as indicated by reductions in microstructural measures or increases in iron deposition, would correlate with RAVLT delayed recall score in the older adult group. The influence of SNpc microstructure on memory was assessed by correlating mean SNpc microstructure and compositional indices with RAVLT delayed recall scores separately in younger and older adults. Age group differences in the magnitude of these relationships were assessed using one-tailed Fisher's *z* tests for independent correlations.

3. Results

3.1 LC microstructure

Figure 3A shows comparison of mean FA in young (i) and older (ii) groups. Age group differences in DTI indices and R_2* were assessed using between-group t-tests. Results revealed reductions in mean LC MD (older: 3.30×10^{-4} mm^2/s $\pm4.27\times10^{-5}$ mm^2/s; young:

3.58×10^{-4} mm^2/s $\pm3.84\times10^{-5}$ mm^2/s; t=2.52; p=0.007), LC RD (older: 2.73×10^{-4} mm^2/s $\pm3.93\times10^{-5}$ mm^2/s; young: 3.06×10^{-4} mm^2/s $\pm3.49\times10^{-5}$ mm^2/s; t=2.64; p=0.005), and LC AD (older: 4.32×10^{-4} mm^2/s $\pm5.36\times10^{-5}$ mm^2/s; young: 4.57×10^{-4} mm^2/s $\pm4.41\times10^{-5}$ mm^2/s; t=1.79; p=0.04) in the older adult cohort relative to the young. An increase in mean LC FA (older: 0.29 ± 0.04; young: 0.27 ± 0.02; t=−2.36; p=0.01) was observed in the older cohort as compared to the young cohort. No difference was observed in mean R_2* in LC between the older and young cohorts (older: 18.2 s^{-1} ± 1.9 s^{-1}; young: 17.4 s^{-1} ± 1.8 s^{-1}; t=−0.88; p=0.07). Group comparisons for LC are summarized in Figure 3.

3.2 LC microstructure and memory

The effect of LC microstructure on memory was assessed by correlating LC diffusion indices (MD, RD, and AD) with RAVLT delayed recall components. In the older adult group mean LC diffusion metrics positively correlate with memory scores (RAVLT delayed recall), indicating that as memory performance increases, LC MD (r=0.618, p=0.001), mean LC RD (r=0.576, p=0.002), and mean LC AD (r=0.637, $p=4.1\times10^{-4}$) also increase. These correlations are shown in Figure 4.

Interestingly, no correlation between any LC diffusion measures and RAVLT delayed recall score was observed in the young group (mean LC MD: r=0.074, p=0.487; mean LC RD: r=0.006, p=0.346; mean LC AD: r=0.119, p=0.262). Moreover, Fisher's z tests revealed that these relationships were significantly smaller in the young compared to older group for all LC diffusion measures (mean LC MD: z=2.236, p=0.013; mean LC RD: z=2.187, p=0.014; mean LC AD: z=2.246, p=0.012).

3.3 SNpc microstructure and composition

SNpc microstructure was assessed using iron sensitive (monopolar; high resolution) and iron insensitive (bipolar; lower resolution with 1.7 mm isotropic voxel) diffusion-weighted acquisitions. Figure 5 shows mean SNpc FA from the high resolution (iron sensitive) acquisition in young (i) and older adult (ii) cohorts, respectively. In the iron sensitive acquisition, reductions in mean SNpc MD (t=3.22; p=0.002), mean SNpc RD (t=2.98; p=0.004), and mean SNpc AD (t=3.09; p=0.002) were observed in the older cohort as compared to the young. A trend toward increased FA was observed in the older cohort (t=−1.43; p=0.08). In the iron insensitive diffusion acquisition, in the older cohort, reductions in MD (t=2.57; p=0.009) and AD (t=3.07; p=0.002) were observed and trends toward decreased RD (t=2.17; p=0.10) and decreased FA (t=−1.37; p=0.06) were seen. Group comparisons for SNpc diffusion markers are detailed in Table 2.

Changes in SNpc composition were assessed using iron sensitive contrasts, and Figure 5 (iii) and (iv) show mean SNpc R_2* in young and older adult cohorts, respectively. An increase in R_2* (older: 32.4 s^{-1}± 5.9s^{-1}; young: 24.6 s^{-1}±2.6 s^{-1}; t=−5.87; $p<10^{-5}$) as well as susceptibility (older: 0.096 ppm ± 0.04 ppm; young: 0.06 ppm ± 0.03 ppm; t=−4.09; $p=1.0\times10^{-4}$) was observed in SNpc of the older adult cohort.

No correlations between age and diffusion indices in SNpc were observed in the older adult cohort (FA: p=0.656; MD: p=0.925; RD: p=0.912) or in the young cohort (FA: p=0.481; MD: p=0.834; RD: p=0.676). A significant correlation was observed between iron in SNpc

and age in the young cohort (R_2*: p=0.008, r=0.462; susceptibility: p=0.01, r=0.445) but no correlation was seen between SNpc iron and age (R_2*: p=0.99, r=0.004; susceptibility: p=0.877, r=−0.111) in the older cohort. Fisher's z tests revealed that these relationships with age were significantly larger in the older compared to young cohort for both iron measures (R_2*: z=1.712, p=0.043; susceptibility: z=2.037, p=0.021).

3.4 SNpc microstructure and memory

We did not see any significant correlations between RAVLT delayed recall and any SNpc measures for either group after multiple comparison correction. In the older group, trends were observed between RAVLT delayed recall and monopolar MD (r=0.278; p=0.11), monopolar AD (r=0.321; p=0.08), monopolar RD (r=0.246; p=0.14), bipolar MD (r=0.323; p=0.077), bipolar AD (r=0.350; p=0.06), and bipolar RD (r=0.298; p=0.095). Similar trends were observed in the young group for the bipolar (MD: r=0.354, p=0.055; RD: r=0.397, p=0.03; AD: r=0.292, p=0.118), but not the monopolar (MD: r=0.095, p=0.306; RD: r=0.025, p=0.446; AD: r=−0.003, p=0.494), SNpc diffusion measures. Fisher's z tests revealed that there were no significant group differences in any of these relationships (ps > 0.14). No significant correlations were observed between RAVLT delayed recall and the iron indices in the older (R_2*: r=−0.144; p=0.266; $\Delta\chi$ (r=−0.161; p=0.243) or young group (R_2*: r=0.105; p=0.288; $\Delta\chi$: r=−0.289; p=0.115). Fisher's z tests revealed that there were no significant group differences in any of these relationships (ps > 0.14).

3.5 Effect of iron of SNpc diffusion measures

Statistically significant correlations were found in the older adult group between iron measures and diffusion measures in SNpc from both acquisitions. Specifically, negative correlations were seen in the older adult group between mean SNpc R_2* all SNpc diffusion measures from the monopolar acquisition (MD: r=−0.638, p=0.001; AD: r=−0.626, p=0.001; RD: r=−0.661, p=0.001) and those from the bipolar acquisition (MD: r=−0.743, $p<10^{-4}$; AD: r=−0.749; $p<10^{-4}$; RD: r=−0.660, p=0.001). These correlations are shown in Figure 6. Correlations of similar strength were observed between mean SNpc $\Delta\chi$ and all SNpc diffusion measures from the monopolar acquisition (MD: r=−0.592, p=0.002; AD: r=−0.586, p=0.002; RD: r=−0.611, p=0.002) and those from the bipolar acquisition (MD: r=−0.782, $p<10^{-4}$; AD: r=−0.724; $p<10^{-4}$; RD: r=−0.772, $p<10^{-4}$).

In the young group, strong negative trends were observed between mean SNpc R_2* and all SNpc diffusion measures from the monopolar acquisition (MD: r=−0.278, p=0.055; AD: r=−0.245, p=0.082; RD: r=−0.259, p=0.070) but no trend was seen between mean SNpc R_2* and any SNpc diffusion measure from the bipolar acquisition (MD: r=−0.025, p=0.444; AD: r=−0.071, p=0.344; RD: r=0.127, p=0.238). However, for SNpc susceptibility, mean SNpc $\Delta\chi$ showed strong negative trends with all SNpc diffusion measures from the monopolar acquisition (MD: r=−0.231, p=0.085; AD: r=−0.207, p=0.118; RD: r=−0.279, p=0.065) as well as with SNpc diffusion measures from the bipolar acquisition (MD: r=−0.432, p=0.011; AD: r=−0.325, p=0.026; RD: r=−0.419, p=0.070).

Fisher's z tests revealed that relationships were significantly stronger in the older compared to young cohort between each SNpc iron index and all SNpc diffusion measures from the

bipolar acquisition (R_2*-MD: z=−3.218, p=0.001; R_2*-AD: z=−3.106, p=0.001; R_2*-RD: z=−3.178, p=0.001; Δχ-MD: z=−2.031, p=0.021; Δχ-AD: z=−1.998, p=0.023; Δχ-RD: z=−1.998, p=0.023). These group differences were significant or trending for diffusion measures from the monopolar acquisition (R_2*-MD: z=−0.62, p=0.053; R_2*-AD: z=−1.88, p=0.03; Δχ-MD: z=−1.538, p=0.062; Δχ-AD: z=−1.594, p=0.056; Δχ-RD: z=−1.464, p=0.072), except for the relationship between SNpc R_2* and monopolar RD (z=−0.011, p=0.496), which did not differ between age groups.

4. Discussion

This study examined the microstructural and compositional differences occurring in catecholamine nuclei during normal aging. In the LC, aging led to expected age-related reductions in diffusivity (MD, RD) and an unexpected increase in anisotropy (FA), but there was no effect of aging on R_2*. Aging in SNpc was accompanied by reductions in diffusivity (but not anisotropy) with additional increases in measures of iron deposition.

The stature of LC is too small for assessment of microstructural changes using traditional diffusion weighted acquisitions, so a high-resolution diffusion weighted acquisition was employed to minimize partial volume effects. We observed increased FA, decreased MD, and decreased RD in LC of the aging cohort as compared to controls. Although diffusion measures can be altered by several microstructural properties, we conjecture that the observed diffusion changes reflect restricted diffusion occurring from a decrease in axon diameter (Barazany et al., 2009; Wheeler-Kingshott and Cercignani, 2009). Prior postmortem studies examining LC have found a reduction in LC cell size of older humans (German et al., 1992). Interestingly, the trend toward increased LC R_2* in the older adult cohort may reflect reduced cell size as tissue compacting or shrinkage increases R_2*. The age-related increase in LC R_2* cannot be attributed to iron deposition as LC neuromelanin granules chelate copper (Sulzer et al., 2018) and neuromelanin is only slightly paramagnetic (Ju et al., 2013).

LC is the primary source of norepinephrine in the brain, and its projections innervate many areas of the brain including regions deeply involved in learning and memory, such as the neocortex and hippocampus (Aston-Jones, G. and Cohen, J. D., 2005). Norepinephrine protects neurons from oxidative stress (Troadec et al., 2001) and reduces inflammation (Feinstein et al., 2002). This protective effect is the basis of the LC-reserve hypothesis by which activation of LC and the release of norepinephrine may offer neuroprotection to neurons innervated by LC (Robertson, 2013). Histological studies found that higher density of neurons in LC correlates with a reduction in cognitive decline (Wilson et al., 2013) and an earlier study found a link between LC contrast and the retention of cognitive reserve (Clewett et al., 2016). Interestingly, we found that lower performance on RAVLT delayed recall scores were correlated with reduced MD and RD (i.e. reduced LC axon size), suggesting that LC microstructure integrity may be important in the retention of cognitive abilities during aging.

Histology has found an age dependence for iron load in substantia nigra (Hallgren and Sourander, 1958), which has been confirmed in several imaging studies (Aquino et al., 2009;

Bilgic et al., 2012; Haacke et al., 2010; Pfefferbaum et al., 2009). Increases in substantia nigra susceptibility, R_2*, or field-dependent relaxation rates have been observed in cohorts of older participants as compared to young participants (Bilgic et al., 2012; Pfefferbaum et al., 2009) and the results presented here accord with these findings. Other work examining iron deposition in a wider age range has been inconclusive with one study finding that iron increases in substantia nigra until early adulthood and then plateaus (Aquino et al., 2009) while another showed iron load increases throughout life (Haacke et al., 2010). Interestingly, results presented here agree with both studies. Specifically, significant positive correlations were seen between SNpc iron measures and age in the young cohort but no significant correlations in iron measures were observed in the older adult cohort, suggesting high accrual rates early in life while group effects suggest iron accrual continues throughout life.

Determination of age-related iron deposition in substantia nigra or its subcomponents (SNpc or substantia nigra pars reticulata) is essential for the establishment of biomarkers to distinguish normal R_2* or QSM values from those due to a pathological condition. For example, in Parkinson's disease, much of the neuronal loss in SNpc occurs prior to symptom onset and increased iron content in substantia nigra is associated with this neuronal loss (Dexter et al., 1991; Wypijewska et al., 2010). However, imaging studies have not reached a consensus regarding nigral iron deposition in Parkinson's disease (Du et al., 2018; Heim et al., 2017; Huddleston et al., 2018; Lehericy et al., 2017), and this inconsistency may be due to placement of substantia ROIs outside SNpc (Langley et al., 2019).

Iron is particularly problematic for diffusion-weighted MRI sequences with monopolar diffusion encoding gradients. Deposits of iron create local magnetic field gradients, which produce cross terms affecting monopolar diffusion encoding gradients and reduce the apparent diffusion coefficient (Novikov et al., 2018; Zhong et al., 1991). Our results from the monopolar diffusion-weighted acquisition accord with this physical model. We found negative correlations between both SNpc iron measures (mean R_2* and mean susceptibility) and diffusivity (MD, AD, and RD) in data acquired with a monopolar diffusion encoding gradient in the older adult group. However, similar correlations were observed in the diffusion-weighted data acquired with a bipolar diffusion encoding gradient. This latter finding is particularly puzzling since physical models suggest bipolar diffusion encoding gradients are insensitive to magnetic field inhomogeneities generated by iron deposits (Fujiwara et al., 2014).

Negative correlations between iron measures and MD as well as positive correlations between FA and iron measures have been observed in the striatum (Pfefferbaum et al., 2010; Syka et al., 2015). These results suggest a complex relationship between iron deposition and diffusivity measures that warrants further study. Specifically, correlations between SNpc susceptibility and diffusion measures from the bipolar acquisition in both groups suggest iron deposition may alter the underlying tissue microstructure or that the correlation between microstructure and iron are incidental and age-related microstructural changes are dominant. Characterization of the relationship between iron and diffusivity is of particular interest in deep gray matter nuclei undergoing age-related or pathologic iron deposition. In particular, this is of interest in the study of PD where iron is deposited in SNpc (Dexter et al., 1987). The development of diagnostic and progression markers for PD has been hindered by

inconsistent results from different studies (Schwarz et al., 2013) and discrepancies in the literature may be partially explained by the sensitivity of diffusion measures to iron content.

Given the negative correlations for diffusion measures and the increase in SNpc iron measures in the older cohort, it is unsurprising that reduced diffusivity was observed in the older cohort. Earlier work examining age-related microstructural differences in substantia nigra found a trend towards reduced MD (p=0.12), a statistically significant reduction in FA, and a statistically significant increase in RD in their older cohort (Vaillancourt et al., 2012). Differences in results between our study and the previous report (Vaillancourt et al., 2012) cannot be attributed to a discrepancy in ROI placement. ROIs were drawn in hypointense regions inferior to red nucleus and were positioned in a spatial location similar to the rostral portion of the neuromelanin-sensitive SN (SNpc) ROI used in this analysis (Langley et al., 2015). Given this, the discrepancy in RD and FA results may be attributed to partial volume effects as their acquisition had a slightly larger voxel size than the diffusion acquisition used in this work.

There are some caveats in the present study. First, although a neuromelanin-sensitive atlas created by our group was applied to these data, neuromelanin-sensitive data were not acquired in the same cohort. Histological data suggests that neuromelanin may be present in LC, but not substantia nigra, at birth (Fenichel and Bazelon, 1968) and neuromelanin accrues in both structures with age (Zecca et al., 2004). Neuromelanin content in both structures peaks around age 60 and decreases later in life (Ma et al., 1999; Manaye et al., 1995; Zecca et al., 2004) with depigmentation of substantia nigra occurring at a rate of 4.7% loss per decade of life (Fearnley and Lees, 1991). Inclusion of neuromelanin-sensitive data would give a holistic assessment of age-related effects. Second, the age distribution of the participants in this study was bimodal, owing to its cross-sectional design, with the mean ages of 20.9 years and 73.5 years for the two populations studied. No participants between the ages of 26 and 60 participated in this study. Third, it is possible that noise may corrupt measurements in SNpc from the high-resolution (monopolar) DTI acquisition. Low SNR from iron deposition or reduced voxel size will negatively bias radial diffusivity but positively bias axial diffusivity, resulting in an increase in FA (Anderson, 2001). We speculate that the effect of noise on the monopolar acquisition is minimal since similar effect sizes are seen in both DTI acquisitions since SNpc SNR in the bipolar acquisition is relatively high (mean SNpc SNR = 82.3). However, additional work is needed to assess the contribution of noise on diffusion indices in iron containing structures. Fourth, given the size of LC, partial volume effects or pulsation may influence LC diffusion measurements. Finally, although participants were screened for self-reported neurological conditions prior to enrollment, it is impossible to exclude the possibility that some of the healthy controls in the older adult cohort have an undiagnosed neurological condition. As mentioned above, LC and SNpc are profoundly effected in the prodromal stages of Alzheimer’s disease (LC only) or PD (LC and SNpc) (Braak et al., 2011; Braak et al., 2003).

5. Conclusion

In this work, a high-resolution diffusion-weighted MRI protocol and a multi-echo gradient echo protocol were employed to examine age-related microstructural and compositional

differences in LC and SNpc. We speculate that older age was most associated with axonal thinning in LC whereas age-related differences in SNpc are likely due to increased iron content. Further, these differences in iron content were found to strongly correlate with diffusion measurements in SNpc in the older adult cohort while strong trends were observed between susceptibility and diffusion in the young cohort.

Acknowledgements

Xiaoping Hu receives support from the Michael J. Fox Foundation (MJF 10854). This work was also supported by R00 AG047334 (Bennett) and R21 AG054804 (Bennett) from the National Institutes of Health/National Institute on Aging. The authors would like to thank Mrs. Chelsea Evelyn for help with data acquisition.

References

Anderson AW, 2001 Theoretical analysis of the effects of noise on diffusion tensor imaging. Magn Reson Med 46(6), 1174–1188. [PubMed: 11746585]

Andersson JL, Skare S, Ashburner J, 2003 How to correct susceptibility distortions in spin-echo echo-planar images: application to diffusion tensor imaging. NeuroImage 20(2), 870–888. [PubMed: 14568458]

Andersson JLR, Sotiropoulos SN, 2016 An integrated approach to correction for off-resonance effects and subject movement in diffusion MR imaging. Neuroimage 125, 1063–1078. [PubMed: 26481672]

Aquino D, Bizzi A, Grisoli M, Garavaglia B, Bruzzone MG, Nardocci N, Savoiardo M, Chiapparini L, 2009 Age-related iron deposition in the basal ganglia: quantitative analysis in healthy subjects. Radiology 252(1), 165–172. [PubMed: 19561255]

Arnsten AF, Contant TA, 1992 Alpha-2 adrenergic agonists decrease distractibility in aged monkeys performing the delayed response task. Psychopharmacology (Berl) 108(1-2), 159–169. [PubMed: 1357704]

Aston-Jones G, Cohen JD, 2005 Adaptive gain and the role of the locus coeruleus-norepinephrine system in optimal performance. J Comp Neurol 493(1), 99–110. [PubMed: 16254995]

Aston-Jones G, Cohen JD, 2005 An integrative theory of locus coeruleus-norepinephrine function: adaptive gain and optimal performance. Annu Rev Neurosci 28, 403–450. [PubMed: 16022602]

Barazany D, Basser PJ, Assaf Y, 2009 In vivo measurement of axon diameter distribution in the corpus callosum of rat brain. Brain 132(Pt 5), 1210–1220. [PubMed: 19403788]

Bartus RT, 1979 Four stimulants of the central nervous system: effects on short-term memory in young versus aged monkeys. J Am Geriatr Soc 27(7), 289–297. [PubMed: 36423]

Beaulieu C, 2002 The basis of anisotropic water diffusion in the nervous system - a technical review. NMR Biomed 15(7-8), 435–455. [PubMed: 12489094]

Bilgic B, Pfefferbaum A, Rohlfing T, Sullivan EV, Adalsteinsson E, 2012 MRI estimates of brain iron concentration in normal aging using quantitative susceptibility mapping. Neuroimage 59(3), 2625–2635. [PubMed: 21925274]

Braak H, Thal DR, Ghebremedhin E, Del Tredici K, 2011 Stages of the pathologic process in Alzheimer disease: age categories from 1 to 100 years. Journal of neuropathology and experimental neurology 70(11), 960–969. [PubMed: 22002422]

Braak H, Tredici KD, Rub U, de Vos RAI, Jansen Steur ENH, Braak E, 2003 Staging of brain pathology related to sporadic Parkinson's disease. Neurobiol Aging 24(2), 197–211. [PubMed: 12498954]

Carter ME, Yizhar O, Chikahisa S, Nguyen H, Adamantidis A, Nishino S, Deisseroth K, de Lecea L, 2010 Tuning arousal with optogenetic modulation of locus coeruleus neurons. Nat Neurosci 13(12), 1526–1533. [PubMed: 21037585]

Chen X, Huddleston DE, Langley J, Ahn S, Barnum CJ, Factor SA, Levey AI, Hu X, 2014 Simultaneous imaging of locus coeruleus and substantia nigra with a quantitative neuromelanin MRI approach. Magn Reson Imaging 32(10), 1301–1306. [PubMed: 25086330]

Clewett DV, Lee TH, Greening S, Ponzio A, Margalit E, Mather M, 2016 Neuromelanin marks the spot: identifying a locus coeruleus biomarker of cognitive reserve in healthy aging. Neurobiol Aging 37, 117–126. [PubMed: 26521135]

Dexter DT, Carayon A, Javoy-Agid F, Agid Y, Wells FR, Daniel SE, Lees AJ, Jenner P, Marsden CD, 1991 Alterations in the levels of iron, ferritin and other trace metals in Parkinson's disease and other neurodegenerative diseases affecting the basal ganglia. Brain 114 (Pt 4), 1953–1975. [PubMed: 1832073]

Dexter DT, Wells FR, Agid F, Agid Y, Lees AJ, Jenner P, Marsden CD, 1987 Increased nigral iron content in postmortem parkinsonian brain. Lancet 2(8569), 1219–1220. [PubMed: 2890848]

Du G, Lewis MM, Sica C, He L, Connor JR, Kong L, Mailman RB, Huang X, 2018 Distinct progression pattern of susceptibility MRI in the substantia nigra of Parkinson's patients. Mov Disord.

Duzel S, Schutze H, Stallforth S, Kaufmann J, Bodammer N, Bunzeck N, Munte TF, Lindenberger U, Heinze HJ, Duzel E, 2008 A close relationship between verbal memory and SN/VTA integrity in young and older adults. Neuropsychologia 46(13), 3042–3052. [PubMed: 18601938]

Fearnley JM, Lees AJ, 1991 Ageing and Parkinson's disease: substantia nigra regional selectivity. Brain 114 (Pt 5), 2283–2301. [PubMed: 1933245]

Feinstein DL, Heneka MT, Gavrilyuk V, Dello Russo C, Weinberg G, Galea E, 2002 Noradrenergic regulation of inflammatory gene expression in brain. Neurochem Int 41(5), 357–365. [PubMed: 12176079]

Fenichel GM, Bazelon M, 1968 Studies on neuromelanin. II. Melanin in the brainstems of infants and children. Neurology 18(8), 817–820. [PubMed: 5692344]

Fujiwara S, Uhrig L, Amadon A, Jarraya B, Le Bihan D, 2014 Quantification of iron in the non-human primate brain with diffusion-weighted magnetic resonance imaging. Neuroimage 102(2), 789–797. [PubMed: 25192653]

German DC, Manaye KF, White CL 3rd, Woodward DJ, McIntire DD, Smith WK, Kalaria RN, Mann DM, 1992 Disease-specific patterns of locus coeruleus cell loss. Ann Neurol 32(5), 667–676. [PubMed: 1449247]

Goldman-Rakic PS, Brown RM, 1981 Regional changes of monoamines in cerebral cortex and subcortical structures of aging rhesus monkeys. Neuroscience 6(2), 177–187. [PubMed: 6111765]

Haacke EM, Miao Y, Liu M, Habib CA, Katkuri Y, Liu T, Yang Z, Lang Z, Hu J, Wu J, 2010 Correlation of putative iron content as represented by changes in R2* and phase with age in deep gray matter of healthy adults. J Magn Reson Imaging 32(3), 561–576. [PubMed: 20815053]

Hallgren B, Sourander P, 1958 The effect of age on the non-haemin iron in the human brain. J Neurochem 3(1), 41–51. [PubMed: 13611557]

Heim B, Krismer F, De Marzi R, Seppi K, 2017 Magnetic resonance imaging for the diagnosis of Parkinson's disease. J Neural Transm (Vienna) 124(8), 915–964. [PubMed: 28378231]

Huddleston DE, Langley J, Dusek P, He N, Faraco CC, Crosson B, Factor S, Hu XP, 2018 Imaging parkinsonian pathology in substantia nigra with MRI. Curr Radiol Rep 6, 15.

Jackson WJ, Buccafusco JJ, 1991 Clonidine enhances delayed matching-to-sample performance by young and aged monkeys. Pharmacol Biochem Behav 39(1), 79–84. [PubMed: 1924516]

Jahanshahi M, Jones CR, Dirnberger G, Frith CD, 2006 The substantia nigra pars compacta and temporal processing. J Neurosci 26(47), 12266–12273. [PubMed: 17122052]

Jenkinson M, Bannister P, Brady M, Smith S, 2002 Improved optimization for the robust and accurate linear registration and motion correction of brain images. NeuroImage 17(2), 825–841. [PubMed: 12377157]

Jenkinson M, Smith S, 2001 A global optimisation method for robust affine registration of brain images. Med Image Anal 5(2), 143–156. [PubMed: 11516708]

Ju KY, Lee JW, Im GH, Lee S, Pyo J, Park SB, Lee JH, Lee JK, 2013 Bio-inspired, melanin-like nanoparticles as a highly efficient contrast agent for T1-weighted magnetic resonance imaging. Biomacromolecules 14(10), 3491–3497. [PubMed: 23987128]

Langkammer C, Schweser F, Krebs N, Deistung A, Goessler W, Scheurer E, Sommer K, Reishofer G, Yen K, Fazekas F, Ropele S, Reichenbach JR, 2012 Quantitative susceptibility mapping (QSM) as

a means to measure brain iron? A post mortem validation study. Neuroimage 62(3), 1593–1599. [PubMed: 22634862]

Langley J, He N, Huddleston DE, Chen S, Yan F, Crosson B, Factor S, Hu X, 2019 Reproducible detection of nigral iron deposition in 2 Parkinson's disease cohorts. Mov Disord 34(3), 416–419. [PubMed: 30597635]

Langley J, Huddleston DE, Chen X, Sedlacik J, Zachariah N, Hu X, 2015 A multicontrast approach for comprehensive imaging of substantia nigra. Neuroimage 112, 7–13. [PubMed: 25731994]

Langley J, Huddleston DE, Merritt M, Chen X, McMurray R, Silver M, Factor SA, Hu X, 2016 Diffusion tensor imaging of the substantia nigra in Parkinson's disease revisited. Hum Brain Mapp 37(7), 2547–2556. [PubMed: 27029026]

Langley J, Huddleston DE, Sedlacik J, Boelmans K, Hu XP, 2017 Parkinson's disease-related increase of T2*-weighted hypointensity in substantia nigra pars compacta. Mov Disord 32(3), 441–449. [PubMed: 28004859]

Langley J, Zhao Q, 2009 Unwrapping magnetic resonance phase maps with Chebyshev polynomials. Magn Reson Imaging 27(9), 1293–1301. [PubMed: 19574009]

Lehericy S, Vaillancourt DE, Seppi K, Monchi O, Rektorova I, Antonini A, McKeown MJ, Masellis M, Berg D, Rowe JB, Lewis SJG, Williams-Gray CH, Tessitore A, Siebner HR, International P, Movement Disorder Society -Neuroimaging Study, G., 2017 The role of high-field magnetic resonance imaging in parkinsonian disorders: Pushing the boundaries forward. Mov Disord 32(4), 510–525. [PubMed: 28370449]

Li W, Wang N, Yu F, Han H, Cao W, Romero R, Tantiwongkosi B, Duong TQ, Liu C, 2015 A method for estimating and removing streaking artifacts in quantitative susceptibility mapping. Neuroimage 108, 111–122. [PubMed: 25536496]

Li W, Wu B, Liu C, 2011 Quantitative susceptibility mapping of human brain reflects spatial variation in tissue composition. NeuroImage 55(4), 1645–1656. [PubMed: 21224002]

Ma SY, Roytt M, Collan Y, Rinne JO, 1999 Unbiased morphometrical measurements show loss of pigmented nigral neurones with ageing. Neuropathol Appl Neurobiol 25(5), 394–399. [PubMed: 10564529]

Manaye KF, McIntire DD, Mann DM, German DC, 1995 Locus coeruleus cell loss in the aging human brain: a non-random process. J Comp Neurol 358(1), 79–87. [PubMed: 7560278]

Novikov DS, Reisert M, Kiselev VG, 2018 Effects of mesoscopic susceptibility and transverse relaxation on diffusion NMR. J Magn Reson 293, 134–144. [PubMed: 30012279]

Pfefferbaum A, Adalsteinsson E, Rohlfing T, Sullivan EV, 2009 MRI estimates of brain iron concentration in normal aging: comparison of field-dependent (FDRI) and phase (SWI) methods. Neuroimage 47(2), 493–500. [PubMed: 19442747]

Pfefferbaum A, Adalsteinsson E, Rohlfing T, Sullivan EV, 2010 Diffusion tensor imaging of deep gray matter brain structures: effects of age and iron concentration. Neurobiol Aging 31(3), 482–493. [PubMed: 18513834]

Robertson IH, 2013 A noradrenergic theory of cognitive reserve: implications for Alzheimer's disease. Neurobiol Aging 34(1), 298–308. [PubMed: 22743090]

Sasaki M, Shibata E, Tohyama K, Takahashi J, Otsuka K, Tsuchiya K, Takahashi S, Ehara S, Terayama Y, Sakai A, 2006 Neuromelanin magnetic resonance imaging of locus ceruleus and substantia nigra in Parkinson's disease. Neuroreport 17(11), 1215–1218. [PubMed: 16837857]

Schwarz ST, Abaei M, Gontu V, Morgan PS, Bajaj N, Auer DP, 2013 Diffusion tensor imaging of nigral degeneration in Parkinson's disease: A region-of-interest and voxel-based study at 3 T and systematic review with meta-analysis. Neuroimage Clin 3, 481–488. [PubMed: 24273730]

Schwarz ST, Rittman T, Gontu V, Morgan PS, Bajaj N, Auer DP, 2011 T1-Weighted MRI shows stage-dependent substantia nigra signal loss in Parkinson's disease. Mov Disord 26(9), 1633–1638. [PubMed: 21491489]

Schweser F, Deistung A, Lehr BW, Reichenbach JR, 2011 Quantitative imaging of intrinsic magnetic tissue properties using MRI signal phase: an approach to in vivo brain iron metabolism? NeuroImage 54(4), 2789–2807. [PubMed: 21040794]

Smith SM, 2002 Fast robust automated brain extraction. Hum Brain Mapp 17(3), 143–155. [PubMed: 12391568]

Smith SM, Jenkinson M, Woolrich MW, Beckmann CF, Behrens TE, Johansen-Berg H, Bannister PR, De Luca M, Drobnjak I, Flitney DE, Niazy RK, Saunders J, Vickers J, Zhang Y, De Stefano N, Brady JM, Matthews PM, 2004 Advances in functional and structural MR image analysis and implementation as FSL. NeuroImage 23 Suppl 1, S208–219. [PubMed: 15501092]

Sulzer D, Cassidy C, Horga G, Kang UJ, Fahn S, Casella L, Pezzoli G, Langley J, Hu XP, Zucca FA, Isaias IU, Zecca L, 2018 Neuromelanin detection by magnetic resonance imaging (MRI) and its promise as a biomarker for Parkinson's disease. NPJ Parkinsons Dis 4, 11. [PubMed: 29644335]

Syka M, Keller J, Klempir J, Rulseh AM, Roth J, Jech R, Vorisek I, Vymazal J, 2015 Correlation between relaxometry and diffusion tensor imaging in the globus pallidus of Huntington's disease patients. PLoS One 10(3), e0118907. [PubMed: 25781024]

Troadec JD, Marien M, Darios F, Hartmann A, Ruberg M, Colpaert F, Michel PP, 2001 Noradrenaline provides long-term protection to dopaminergic neurons by reducing oxidative stress. J Neurochem 79(1), 200–210. [PubMed: 11595772]

Vaillancourt DE, Spraker MB, Prodoehl J, Zhou XJ, Little DM, 2012 Effects of aging on the ventral and dorsal substantia nigra using diffusion tensor imaging. Neurobiol Aging 33(1), 35–42. [PubMed: 20359780]

Wheeler-Kingshott CA, Cercignani M, 2009 About "axial" and "radial" diffusivities. Magn Reson Med 61(5), 1255–1260. [PubMed: 19253405]

Wilson RS, Nag S, Boyle PA, Hizel LP, Yu L, Buchman AS, Schneider JA, Bennett DA, 2013 Neural reserve, neuronal density in the locus ceruleus, and cognitive decline. Neurology 80(13), 1202–1208. [PubMed: 23486878]

Woolrich MW, Jbabdi S, Patenaude B, Chappell M, Makni S, Behrens T, Beckmann C, Jenkinson M, Smith SM, 2009 Bayesian analysis of neuroimaging data in FSL. NeuroImage 45(1 Suppl), S173–186. [PubMed: 19059349]

Wypijewska A, Galazka-Friedman J, Bauminger ER, Wszolek ZK, Schweitzer KJ, Dickson DW, Jaklewicz A, Elbaum D, Friedman A, 2010 Iron and reactive oxygen species activity in parkinsonian substantia nigra. Parkinsonism & related disorders 16(5), 329–333. [PubMed: 20219408]

Zecca L, Stroppolo A, Gatti A, Tampellini D, Toscani M, Gallorini M, Giaveri G, Arosio P, Santambrogio P, Fariello RG, Karatekin E, Kleinman MH, Turro N, Hornykiewicz O, Zucca FA, 2004 The role of iron and copper molecules in the neuronal vulnerability of locus coeruleus and substantia nigra during aging. Proc Natl Acad Sci U S A 101(26), 9843–9848. [PubMed: 15210960]

Zhong J, Kennan RP, Gore JC, 1991 Effects of susceptibility variations on NMR measurements of diffusion. J Magn Reson 95, 267–280.

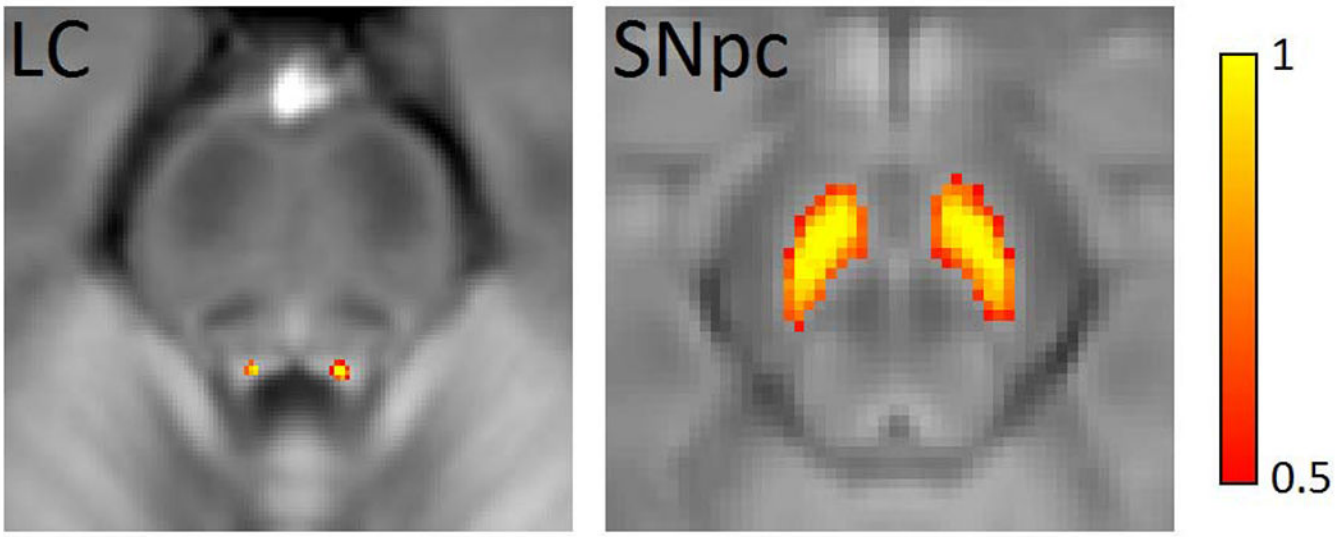

Figure 1.

LC (left) and SNpc (right) masks used to define ROIs in the diffusion, R_2*, and susceptibility analyses overlaid on mean NM-MRI images. LC – locus coeruleus; SNpc – substantia nigra pars compacta; ROIs – regions of interest; NM-MRI – neuromelanin-sensitive MRI.

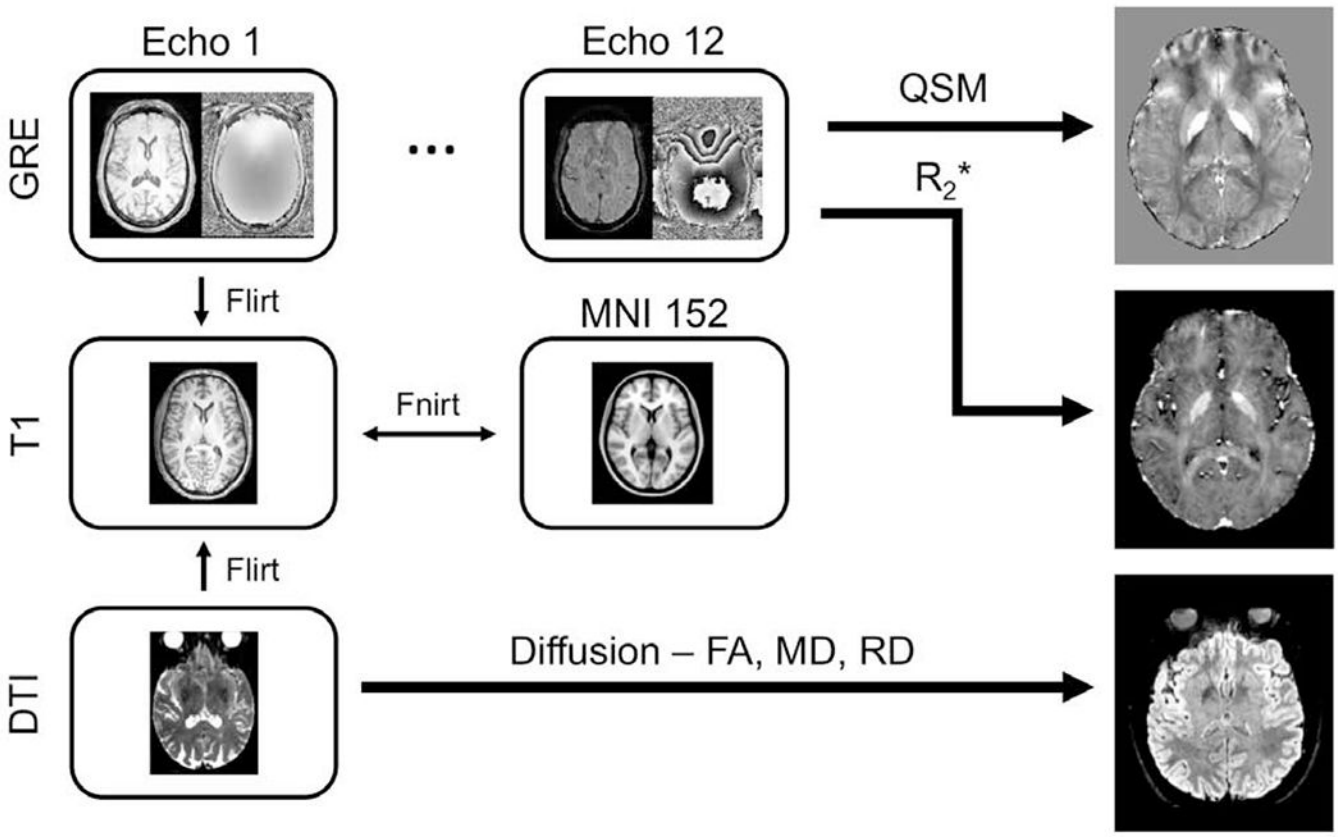

Figure 2.

The registration and processing pipeline. QSM and R_2* images were created from the phase and magnitude images in the multi-echo GRE acquisition, respectively. FA, MD, and RD images were created from the high resolution diffusion-weighted acquisition. Registration between GRE and T_1 images was derived from the first echo of the GRE acquisition with a rigid body transformation, and registration between diffusion-weighted and T_1 images was derived using the *b*=0 image with a rigid body transformation with boundary based registration cost function. QSM – quantitative susceptibility mapping; MD – mean diffusivity; AD – axial diffusivity; RD – radial diffusivity; FA – fractional anisotropy; GRE – gradient recalled echo.

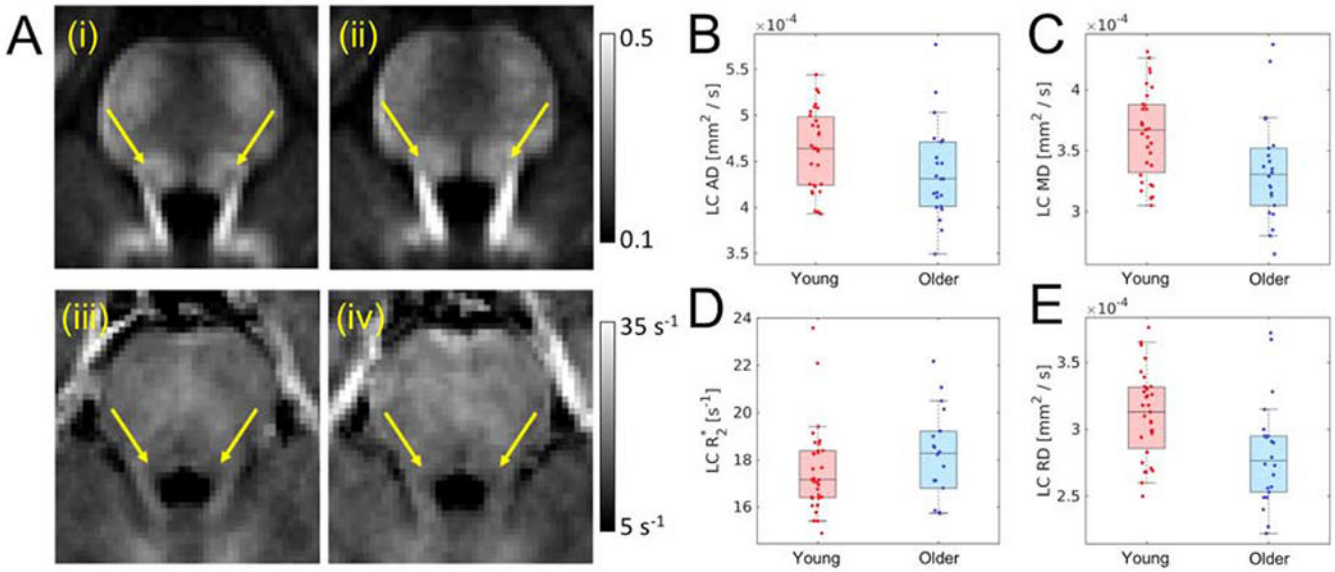

Figure 3.

Part A shows comparison of mean LC FA in young (i) and older adult (ii) cohorts as well as mean R_2* in young (iii) and older adult (iv) cohorts. In A (i-iv) arrows show the approximate location of LC. Group comparisons are shown for AD (B), MD (C), and RD (D), and R_2* (E). A statistically significant increase in mean LC FA was observed in the older cohort while reductions in mean LC RD and mean LC MD were seen in the older cohort. LC – locus coeruleus; MD – mean diffusivity; AD – axial diffusivity; RD – radial diffusivity; FA – fractional anisotropy.

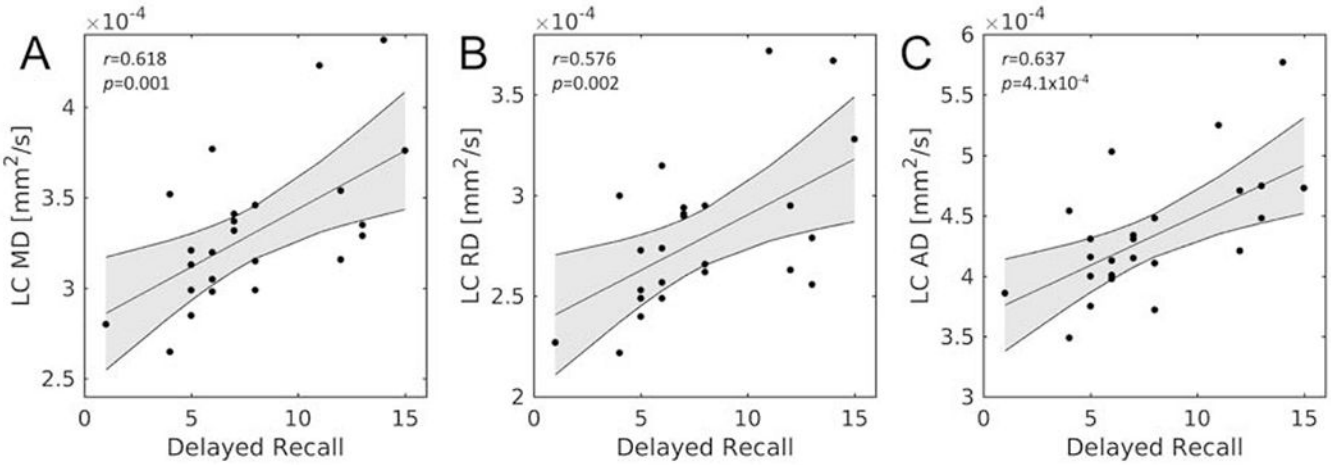

Figure 4.

Correlations between mean LC diffusion measures and RAVLT delayed recall in the older adult group. Statistically significant correlations were observed between mean LC MD (A), mean LC RD (B), and mean LC AD (C) with RAVLT delayed recall. LC – locus coeruleus; MD – mean diffusivity; AD – axial diffusivity; RD – radial diffusivity; FA – fractional anisotropy; RAVLT – Rey Auditory Verbal Learning Test.

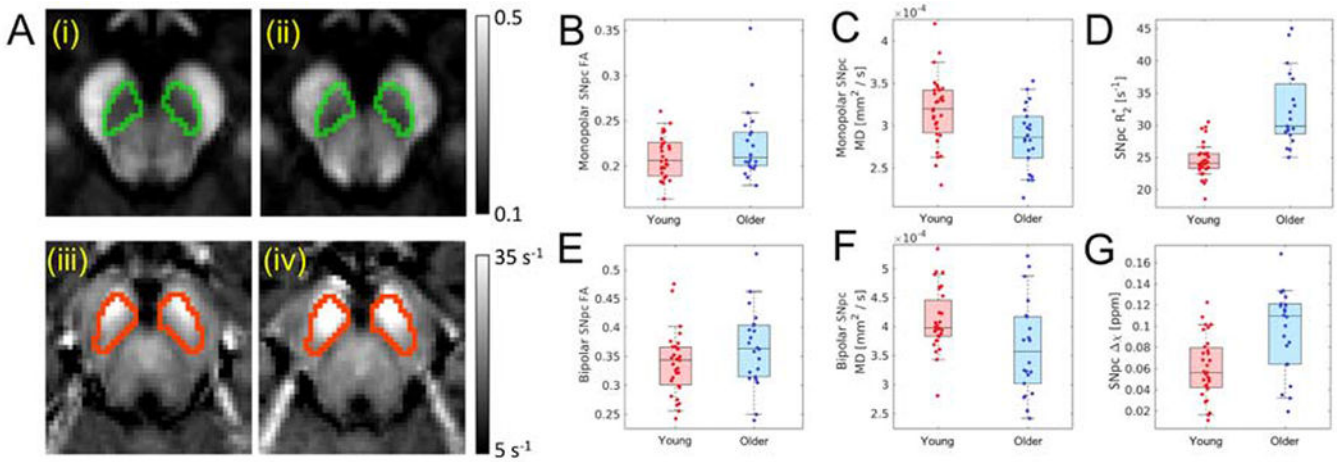

Figure 5.

Part A shows comparison of mean SNpc FA in young (i) and older adult (ii) cohorts as well as mean R_2* in young (iii) and older adult (iv) cohorts. SNpc is outlined in green in mean FA maps (i and ii) and red in mean R_2* maps (iii and iv). Group comparisons are shown for monopolar FA (B) and bipolar FA (E), monopolar MD (C) and bipolar MD (F), R_2* (D), and susceptibility (G). Statistically significant increases in mean SNpc R_2* and susceptibility were observed in the older adult cohort while a reduction in mean SNpc MD were seen in the older adult cohort for monopolar and bipolar DTI acquisitions. SNpc – substantia nigra pars compacta; MD – mean diffusivity; AD – axial diffusivity; RD – radial diffusivity; FA – fractional anisotropy.

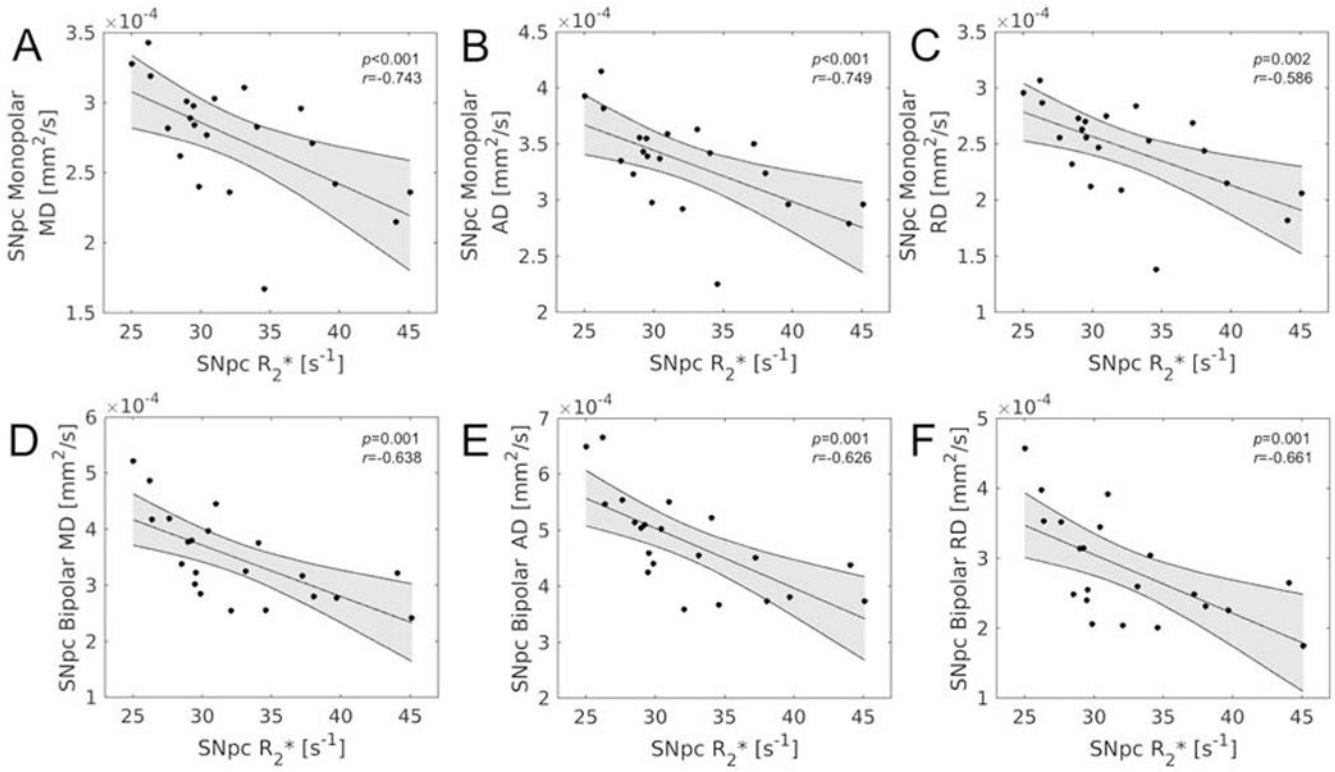

Figure 6.

Correlations between R_2* and diffusion measures in SNpc in the older adult group. Statistically significant correlations were observed between all bipolar diffusion measures (A – SNpc MD, B – SNpc AD, C- SNpc RD) and R_2* as well as between all monopolar diffusion measures (D – SNpc MD, E – SNpc AD, F- SNpc RD) and R_2*. SNpc – substantia nigra pars compacta; MD – mean diffusivity; AD – axial diffusivity; RD – radial diffusivity; FA – fractional anisotropy.

Table 1.

Demographic information for the participant populations used in statistical analysis in this study. Demographic data are presented as mean ± standard deviation. MOCA - Montreal cognitive assessment scoring; RAVLT - Rey Auditory Verbal Learning Test.

Variable	Young (n=35)	Older (n=22)	*p* Value
Gender (M/F)	15/20	9/13	0.414
Age (yrs)	20.7±2.2	73.0±6.7	$<10^{-4}$
MOCA score	26.9±1.9	26.7±1.9	0.78
RAVLT Total	49.8±7.5	42.7±12.4	0.01
RAVLT Immediate	11.5±2.2	7.7±2.2	$<10^{-4}$
RAVLT Delay	11.1±2.5	8.0±3.8	0.0007

Table 2.

Summary of SNpc diffusion markers from the monopolar (iron sensitive) and bipolar diffusion acquisitions (iron insensitive). Data are presented as mean ± standard deviation MD – mean diffusivity; AD – axial diffusivity; RD – radial diffusivity; FA – fractional anisotropy.

SNpc Marker	Monopolar Diffusion Encoding Gradient			Bipolar Diffusion Encoding Gradient		
	Young	Older	*p* Value	Young	Older	*p* Value
MD [mm^2/s]	$3.2\times10^{-4}\pm4.1\times10^{-5}$	$2.9\times10^{-4}\pm3.8\times10^{-5}$	0.001	$4.1\times10^{-4}\pm5.3\times10^{-5}$	$3.6\times10^{-4}\pm8.0\times10^{-5}$	0.009
AD [mm^2/s]	$3.4\times10^{-4}\pm4.5\times10^{-5}$	$3.7\times10^{-4}\pm3.8\times10^{-5}$	0.002	$5.6\times10^{-4}\pm6.4\times10^{-5}$	$4.8\times10^{-4}\pm9.8\times10^{-5}$	0.002
RD [mm^2/s]	$2.8\times10^{-4}\pm3.7\times10^{-5}$	$2.5\times10^{-4}\pm3.6\times10^{-5}$	0.004	$3.4\times10^{-4}\pm5.2\times10^{-5}$	$3.0\times10^{-4}\pm7.6\times10^{-5}$	0.10
FA	0.29 ± 0.04	0.27 ± 0.02	0.06	0.34 ± 0.05	0.36 ± 0.07	0.06